Applied Catalysis B: Environment and Energy 349 (2024) 123895

Contents lists available at ScienceDirect

Applied Catalysis B: Environment and Energy

journal homepage: www.elsevier.com/locate/apcatb

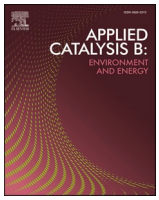

Engineering heteropolyblue hole transfer layer for efficient photoelectrochemical water splitting of $BiVO_4$ photoanodes

Lei Gan [a], GaoShuang He [a], Yang Liu [a], Wenzhang Li [a,b,*], Jie Li [a,**]

[a] School of Chemistry and Chemical Engineering, Central South University, Changsha 410083, China
[b] Hunan Provincial Key Laboratory of Chemical Power Sources, Central South University, Changsha, 410083, China

ARTICLE INFO

Keywords:
Hole transfer layer
Heteropolyblue
$BiVO_4$
Photoelectrochemical water splitting

ABSTRACT

Constructing hole transport layer (HTL) has emerged as a forefront approach to enhance the efficiency of photoelectrochemical (PEC) water oxidation. Here, we introduce the concept of the heteropolyblue HTL as a solution to address the orientation anisotropy issue associated with traditional solid-phase HTL. Integrated with cobalt-based polyoxometalate oxygen evolution cocatalyst and $BiVO_4$ substrate, a $BiVO_4$/HPMo: Co photoanode was constructed, achieving a separation efficiency of 96% and a photocurrent density of 5.7 mA cm^{-2} at 1.23 V vs. RHE. Combined with the calculation results, we determined that the Mo^{6+}/Mo^{5+} electron pair in heteropolyblue acts as a bridge for hole transport. The robust redox capabilities and electron-rich characteristics of heteropolyblue confer durability to the HTL and enable the continuous transport of holes, collectively expediting reaction kinetics. This work represents the initial exploration of the systematic integration of heteropolyblue with photoanodes, unveiling the considerable potential of heteropolyblue in PEC systems.

1. Introduction

Photoelectrochemical (PEC) water splitting has garnered significant attention as a prospective strategy for addressing energy and environmental concerns [1]. However, the realization of efficient PEC water splitting relies on the development of semiconductor photoanodes capable of wide light absorption range, efficient charge separation, facile fabrication processes and enhanced surface reactivity [2]. To this end, a wide range of semiconductor materials, including Fe_2O_3 [3], TiO_2 [4], WO_3 [5], GaP [6], $BiVO_4$ [7], and TaON [8], have been explored as potential candidates for photoanodes. Among these options, $BiVO_4$ has garnered particular attention owing to its favorable bandgap and cost-effectiveness [9]. Nevertheless, issues such as limited charge transport and increased charge recombination in $BiVO_4$ photoanodes have restricted their PEC performance, resulting in photocurrent densities significantly below theoretical projections [10,11]. Consequently, various strategies have been explored to enhance the PEC performance of $BiVO_4$ photoanodes, including elemental doping [12], heterostructure building [13], and morphology engineering [14], etc. While these efforts have improved carrier mobility and electrical conductivity, the challenge of inefficient hole transfer persists, significantly impeding the overall conversion efficiency of the photoelectrode [15–18].

The establishment of HTL stands as a forefront strategy for enhancing the water oxidation efficiency in PEC systems [19,20]. Noteworthy candidates for HTLs, such as certain transition metal oxides [21,22] and carbonitrides [23], have demonstrated substantial potential and yielding remarkable outcomes. Although the utilization of HTLs for enhancing PEC water oxidation has proven effective, the ideal HTL should exhibit uniform adhesion to the photoanode substrate, ensuring the shortest possible migration distance for all holes. Traditional HTL photoanode systems are characterized by non-uniform associations between solid phases, with a significant presence of grain boundary barriers within the solid phase. This anisotropic orientation imposes a requirement for holes to possess higher energy for transmission, consequently impeding hole transfer efficiency.

Polyoxometalates (POMs) are a class of compounds comprising transition metals and oxygen atoms [24]. A well-defined molecular structure is particularly attractive for the precise regulation of water oxidation reactivity at the molecular level [25]. Heteropolyblue, distinguished by its robust electron delocalization, represents a reduced form of POMs, maintaining its structural integrity even during repeated multi-electron redox transitions [26]. Moreover, heteropolyblue

* Corresponding author at: School of Chemistry and Chemical Engineering, Central South University, Changsha 410083, China.
** Corresponding author.
E-mail addresses: liwenzhang@csu.edu.cn (W. Li), lijieliu@csu.edu.cn (J. Li).

https://doi.org/10.1016/j.apcatb.2024.123895
Received 27 November 2023; Received in revised form 27 January 2024; Accepted 26 February 2024
Available online 27 February 2024

exhibits a straightforward synthesis process, high water solubility, and facilitates the straightforward fabrication of device films, typically featuring a spherical structure with dimensions in the nanometer range [27]. This quasi-isotropic structure promotes excellent intramolecular carrier transport with the photoelectrode [28]. Drawing inspiration from these features, the utilization of the isotropic water-soluble heteropolyblue HTL is expected to overcome the limitations of conventional solid-state HTL, which is being considered for finely tuning hole transfer, offering significant promise for practical PEC applications. However, to the best of our knowledge, there are few studies on the application of heteropolyblue HTL in the field of PEC water oxidation.

Herein, we developed a simple and efficient blade-coating strategy to design water-soluble heteropolyblue HTL (HPMO: Sn) synthesized from facile mixing of $H_3PMo_{12}O_{40}$ (HPMO) and $SnCl_2$. Polyethyleneimine (PEI) is employed as a common anti-cation in the heteropolyblue and oxygen evolution cocatalyst ($[CO_4(H_2O)_2(PW_9O_{34})_2]^{10-}$, Co_4POM) interlayer to stabilize the modified layer. HPMO: Sn forms an electron-rich inorganic macromolecular cluster between the oxygen evolution cocatalyst and the $BiVO_4$ array. The $BiVO_4$/HPMo: Co photoanode achieves a photocurrent density of 5.7 mA cm^{-2} at 1.23 V vs. RHE, which is about 3.97 times that of $BiVO_4$ photoanode. The remarkable hole transport capability of heteropolyblue is attributed to its robust redox properties and stability. Our work signifies the initial exploration of the systematic integration of heteropolyblue with photoanodes, unveiling the considerable potential of heteropolyblue in catalyzing the oxygen evolution reaction in PEC systems. This work not only illustrates the viable application of heteropolyblue as HTL in the realm of PEC technology but also presents a promising approach for the systematic development of photoanode designs.

2. Results and discussion

We employed a straightforward blade-coating strategy approach to fabricate $BiVO_4$/HPMo: Co photoanode arrays, as outlined in Scheme 1. Initially, the $BiVO_4$ arrays were grown on fluorine-doped tin oxide (FTO) glass substrates. Subsequently, the HPMO:Sn HTL was prepared by simply mixing methanolic solutions of HPMO and $SnCl_2$, which were then deposited onto the $BiVO_4$ array using a blade-coated technique. To encapsulate the HPMO: Sn, PEI was employed as an anti-cation. Lastly, the Co_4POM reaction layer, followed by the PEI anti-cation layer, and again by a Co_4POM reaction layer, were sequentially spin-coated, resulting in the formation of the $BiVO_4$/HPMo: Co array after heat treatment.

The morphology and structural features of the $BiVO_4$ photoanodes were investigated through scanning electron microscopy (SEM) and transmission electron microscopy (TEM) before and after modification. Fig. 1a-b depict the worm-like porous structure of the nanoporous $BiVO_4$ photoanodes grown on FTO substrates through electrodeposition and calcination. The morphology of the $BiVO_4$/HPMo: Co photoanode is shown in Fig. 1c-d. Compared to the pristine $BiVO_4$ photoanode, the $BiVO_4$/HPMo: Co photoanode has no obvious morphology change, which is caused by the uniform ultra-thin film structure of the HPMO: Sn HTL and Co_4POM reactive layers closely combined with the $BiVO_4$ array. This observation is further substantiated by the TEM images. As shown in Fig. 1e, the unmodified $BiVO_4$ exhibits a well-defined and homogeneous interfacial structure, whereas the $BiVO_4$/HPMo: Co photoanode interface is covered by an amorphous nanolayer approximately 15–20 nm in thickness (Fig. 1f). This is further elucidated in Fig. 1g, where the surface of the $BiVO_4$/HPMo: Co photoanode exhibits tightly adhered and well-defined nano-amorphous layers corresponding to the substrate $BiVO_4$, the HPMo: Sn HTL, and the surface active layer Co_4POM. This conclusion can be further proven in Fig. S1. The element distribution, depicted in Figs. 1h-i, shows the uniform distribution of all elements on the $BiVO_4$/HPMo: Co photoanode surface. The aforementioned findings collectively demonstrate the remarkable compatibility and surface affinity among the HPMo: Sn HTL, the surface active layer Co_4POM, and the substrate $BiVO_4$.

The structural composition and elemental states of diverse photoanodes were characterized through X-ray diffraction (XRD) and X-ray photoelectron spectroscopy (XPS). The XRD patterns of all photoanodes are illustrated in Fig. 2a. All diffraction peaks for the various arrays are indexed as monoclinic $BiVO_4$ (JCPDS PDF #14-0688) and SnO_2 (JCPDS PDF #41-1445) [29]. For comparison, the PEC activities of pristine $BiVO_4$, HPMo: Sn-decorated $BiVO_4$ photoanodes (marked as $BiVO_4$/HPMo), and Co_4POM-decorated $BiVO_4$ photoanodes (marked as $BiVO_4$/Co_4POM) were also assessed. In contrast to the pristine $BiVO_4$, the other modified photoanodes exhibit no discernible additional diffraction peaks, which can be attributed to the relatively low content of HPMo: Sn and Co_4POM. The FT-IR spectral analysis of Co_4POM (Fig. 2b) demonstrates characteristic peaks at 1022 and 932 cm^{-1}, corresponding to the P-O stretching and terminal W-O_t stretching frequencies, while the features at 881 and 710 cm^{-1} correspond to the W-O_b-W stretching of Co_4POM. These results are consistent with previous reports, indicating the successful preparation of Co_4POM [30]. The elemental state of $BiVO_4$/HPMo: Co were further investigated by XPS technology. Compared with pristine $BiVO_4$, a negative shift of Bi 4 f and V 2p was observed in the $BiVO_4$/HPMo: Co array (Figs. 2c-d), indicating that heteropolyblue HPMo: Sn HTL and the Co_4POM reactive layer induces changes in the electronic structure. Subsequent to the incorporation of the HPMo:Sn HTL, the Mo 3d core level spectrum exhibits distinct double peaks at 231.5 and 234.6 eV, corresponding to Mo^{6+} $3d_{5/2}$ and Mo^{6+} $3d_{3/2}$ (Fig. 2f). Additionally, the presence of Mo^{5+} $3d_{5/2}$ and Mo^{5+} $3d_{3/2}$ states is evident through two peaks at 230.1 and 233.2 eV. These results provide evidence of the effective electron

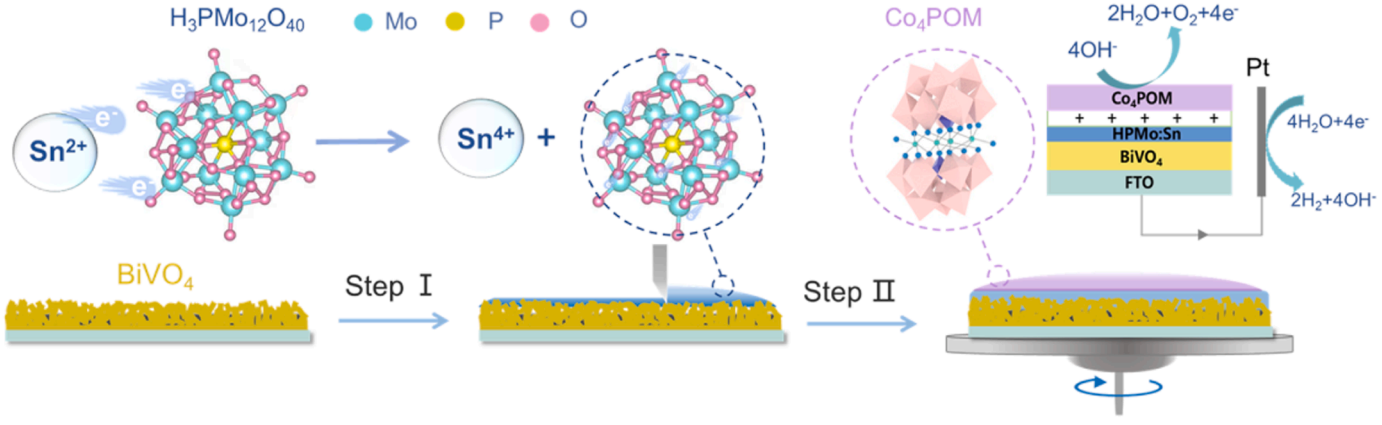

Scheme 1. Schematic illustration of the synthesis process for preparing $BiVO_4$/HPMo: Co arrays by combining HPMO: Sn as the HTL and cobalt-based polyoxometalates as the oxygen evolution cocatalyst.

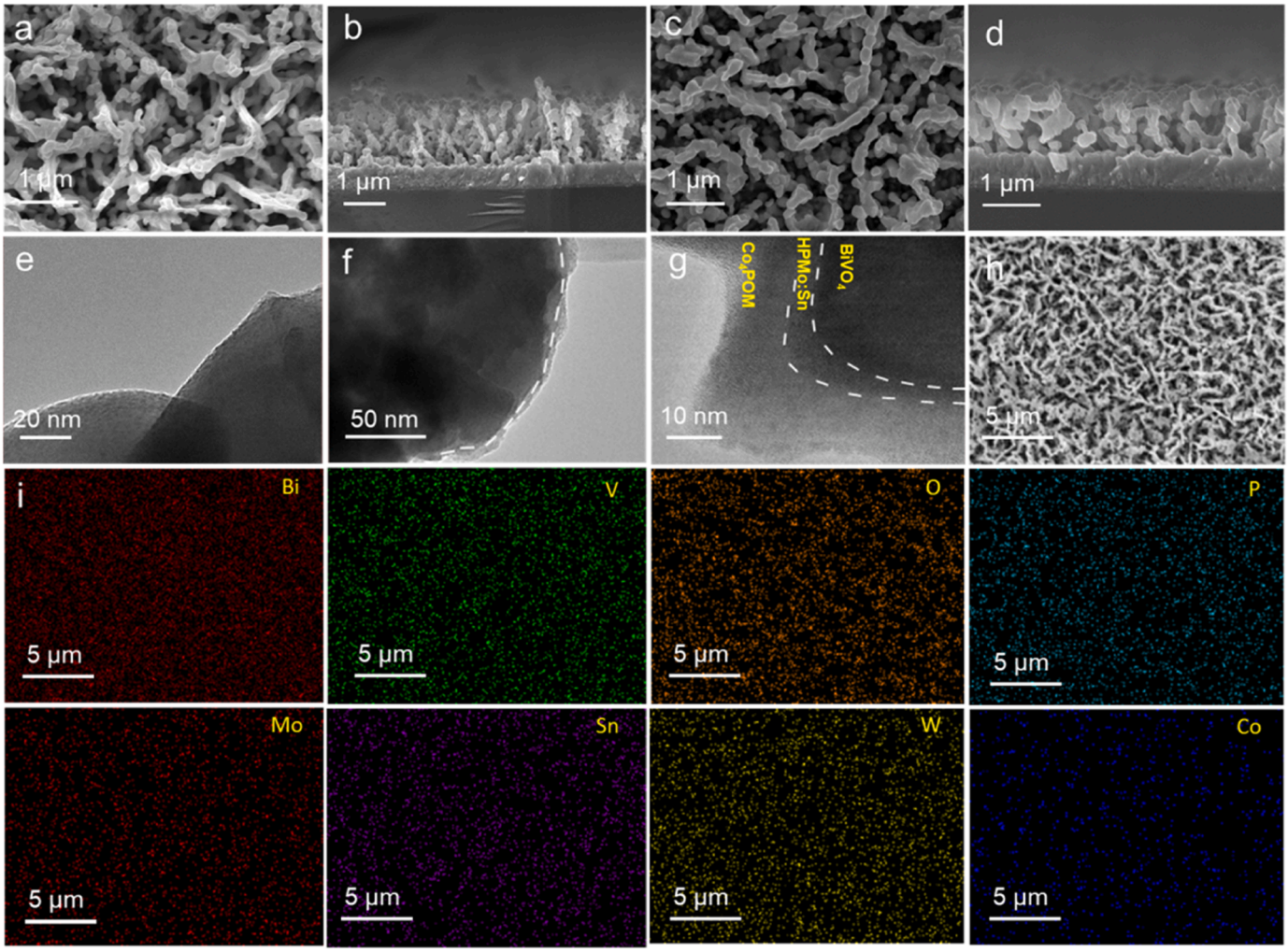

Fig. 1. SEM top-view (a, c) and cross-sectional (b, d) images are presented for (a, b) $BiVO_4$ and (c, d) $BiVO_4$/HPMo: Co. TEM images depict (e) $BiVO_4$. (f, g) $BiVO_4$/HPMo: Co. (i) Element mappings of $BiVO_4$/HPMo: Co corresponding to SEM image of (h) $BiVO_4$/HPMo: Co.

transfer from Sn^{2+} to HPMo, resulting in the partial reduction of Mo^{6+} to Mo^{5+} [31]. This successful process culminates in the fabrication of the $BiVO_4$/HPMo: Co photoanode.

To explore the PEC water splitting performance of all photoanodes, evaluations were performed in three-electrode cells. As depicted in Fig. 3a, the $BiVO_4$/HPMo: Co photoanode demonstrates the highest photocurrent density in comparison to the $BiVO_4$, $BiVO_4$/HPMo, and $BiVO_4$/Co_4POM photoanodes. Specifically, the $BiVO_4$/HPMo: Co photoanode achieves remarkable photocurrent density of 5.7 mA cm^{-2} at 1.23 V vs. RHE, which is approximately 3.97 times higher than that of pristine $BiVO_4$ (1.4 mA cm^{-2}). $BiVO_4$/HPMo and $BiVO_4$/Co_4POM photoanodes also achieve photocurrent densities of 2.52 and 3.13 mA cm^{-2}, respectively. The results above provide evidence of the significant role played by the HPMo: Sn HTL in enhancing the PEC performance of the $BiVO_4$ photoanodes.

In order to optimize the utilization of the HPMo: Sn HTL, the number of active layers of Co_4POM and the heat treatment temperature of $BiVO_4$/HPMo: Co were explored. The results, as shown in Fig. S2, indicate that the $BiVO_4$/HPMo: Co photoanode with 2-layer Co_4POM active layer achieves the highest photocurrent density under heat treatment at 200 °C [32]. Moreover, applied bias photon current efficiency (ABPE) was calculated for all the photoanodes (Fig. 3b). Notably, the $BiVO_4$/HPMo: Co photoanode exhibits a significantly higher ABPE value, reaching 1.83% at 0.66 V vs. RHE. This value surpasses those of the $BiVO_4$/Co_4POM (1.02% at 0.67 V vs. RHE), $BiVO_4$/HPMo (0.38% at 0.92 V vs. RHE), and pristine $BiVO_4$ (0.17% at 0.97 V vs. RHE) photoanodes. Incident photon-to-current conversion efficiency (IPCE) measurements (Fig. 3c) demonstrate that the $BiVO_4$/HPMo: Co photoanode outperforms the others under monochromatic light, highlighting the enhanced photoconversion efficiency achieved through the HPMo: Sn HTL.

To further investigate the capabilities of the HPMo: Sn HTL, all photoanodes were evaluated using Na_2SO_3 as a hole scavenger, and the results were shown in Fig. 3d. Remarkably, the $BiVO_4$/HPMo: Co photoanode achieved a remarkable current density of 6.5 mA cm^{-2} at 1.23 V vs. RHE, surpassing the performance of the other photoanodes. However, the $BiVO_4$/HPMo photoanode did not exhibit a significant improvement in current density, as the surface was coated with PEI, obstructing contact with the sacrificial agent. The charge transfer efficiency (η_{trans}) and charge separation efficiency (η_{sep}) were evaluated (Figs. 3e-f). Compared with the bare $BiVO_4$ photoanode (34%), the $BiVO_4$/HPMo: Co photoanode obtains high charge transfer efficiency (88%), which proves that the HPMo: Sn HTL and the Co_4POM reaction layer significantly improved the photogenerated hole transport and surface reaction kinetics. Strikingly, the $BiVO_4$/HPMo: Co photoanode exhibits an exceptionally high charge separation efficiency of 96%, underscoring the effective separation of photogenerated charge carriers and the suppression of charge recombination by the HPMo: Sn HTL.

Future practical applications demand heteropolyblue HTL with versatility and durability [33–35]. Fig. 3g shows the current-time curves

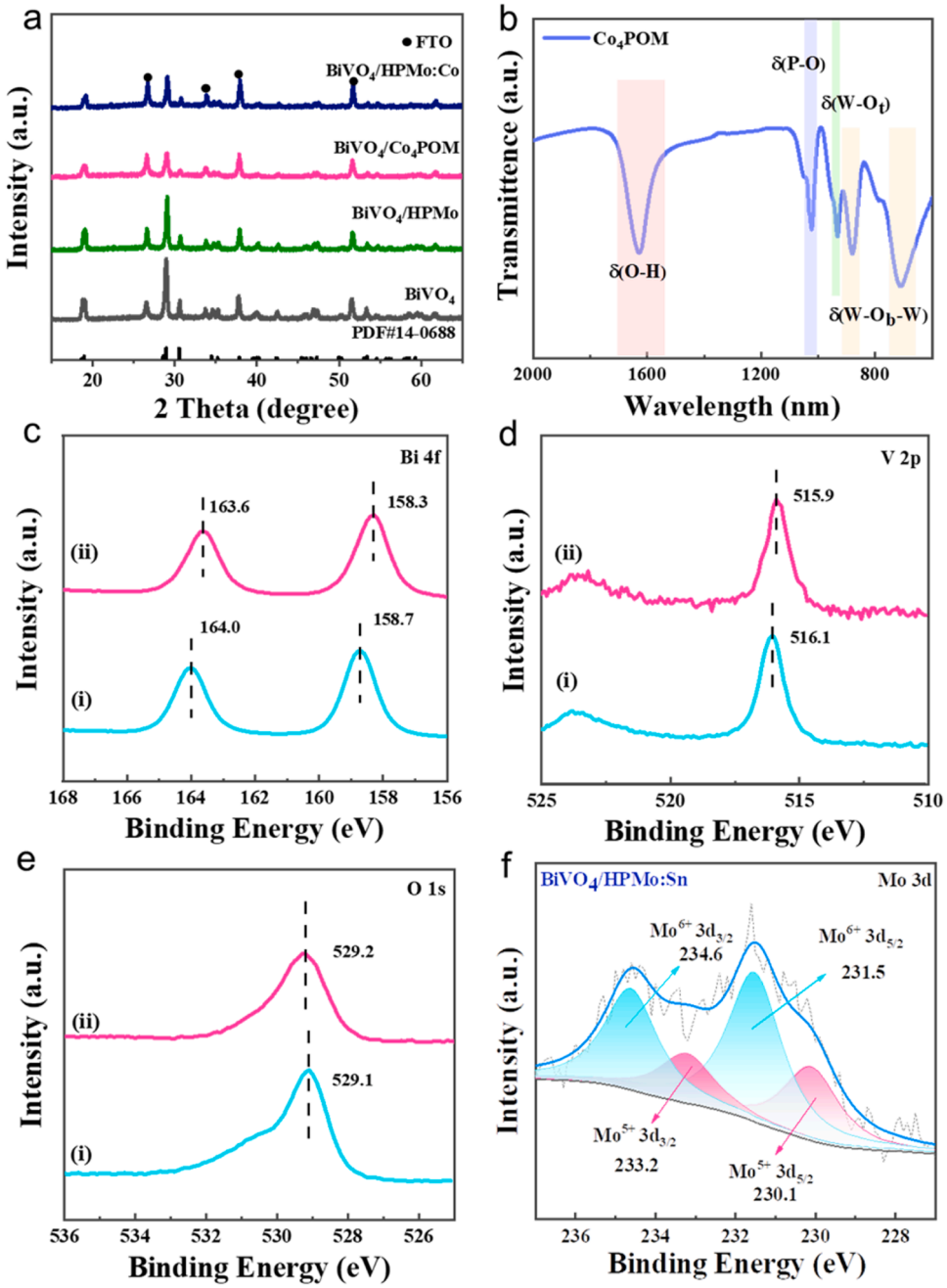

Fig. 2. The XRD patterns (a). (b) FT-IR spectra of Co_4POM. XPS of (c) Bi 4 f. (d) V 2p and (e) O 1 s of (i) $BiVO_4$ and (ii) $BiVO_4$/HPMo: Co. (f) Mo 3d.

of the $BiVO_4$/HPMo: Co photoanode operating at 0.60 V vs. RHE under chopped irradiation. The $BiVO_4$/HPMo: Co photoanode exhibits photocurrent stability throughout the test without significant decay. In contrast, both the current-time curves of the $BiVO_4$/HPMo: Co photoanode and pristine $BiVO_4$ photoanode exhibit continuous decay at 1.23 V vs. RHE, indicating that HPMo: Sn HTL and Co_4POM does not inhibit the photocorrosion of $BiVO_4$ photoanodes at high potentials (Fig. S3a) [36]. Constructing heteropolyblue HPMo: Sn HTL into WO_3 and Ti-Fe_2O_3 photoanodes demonstrated similar advantages, indicating the universality of heteropolyblue HPMo: Sn HTL (Fig. S4). The amount of O_2 produced by the water splitting of PEC on the $BiVO_4$/HPMo: Co photoanode was measured by gas chromatography (GC). After 1 h of irradiation, the amounts of H_2 and O_2 exhibited a linear increase, followed by a gradual rise, ultimately reaching levels of 54.33 and 25.67 μmol, respectively (Fig. S3b). Furthermore, the $BiVO_4$/HPMo: Co photoanode attains an average faradaic efficiency approaching 97%, providing additional confirmation of the exceptional PEC oxygen evolution capability of the $BiVO_4$/HPMo: Co photoanode.

To elucidate the mechanism of $BiVO_4$/HPMo: Co enhanced PEC activity, the optical properties and electrochemical behavior were investigated. There is no significant change in the edge position of the light absorption band for all photoanodes (Fig. S5). Furthermore, steady-state photoluminescence (PL) measurements were performed on $BiVO_4$-based photoanodes. As shown in Fig. 4a, the PL intensity spectrum of the $BiVO_4$/HPMo: Co photoanode is notably lower than that of the other photoanodes, indicating that the $BiVO_4$/HPMo: Co photoanode excels in facilitating charge separation and effectively suppressing electron-hole recombination. Time-resolved transient absorption spectroscopy (TR-TAS) was employed to evaluate the charge carrier lifetime of $BiVO_4$-based photoanodes in the excited state [37]. As shown in Fig. 4b and Table S1, the carrier lifetime of the $BiVO_4$/HPMo: Co photoelectrode (7.01 ns) is longer than that of $BiVO_4$ (2.69 ns), $BiVO_4$/HPMo (4.71 ns),

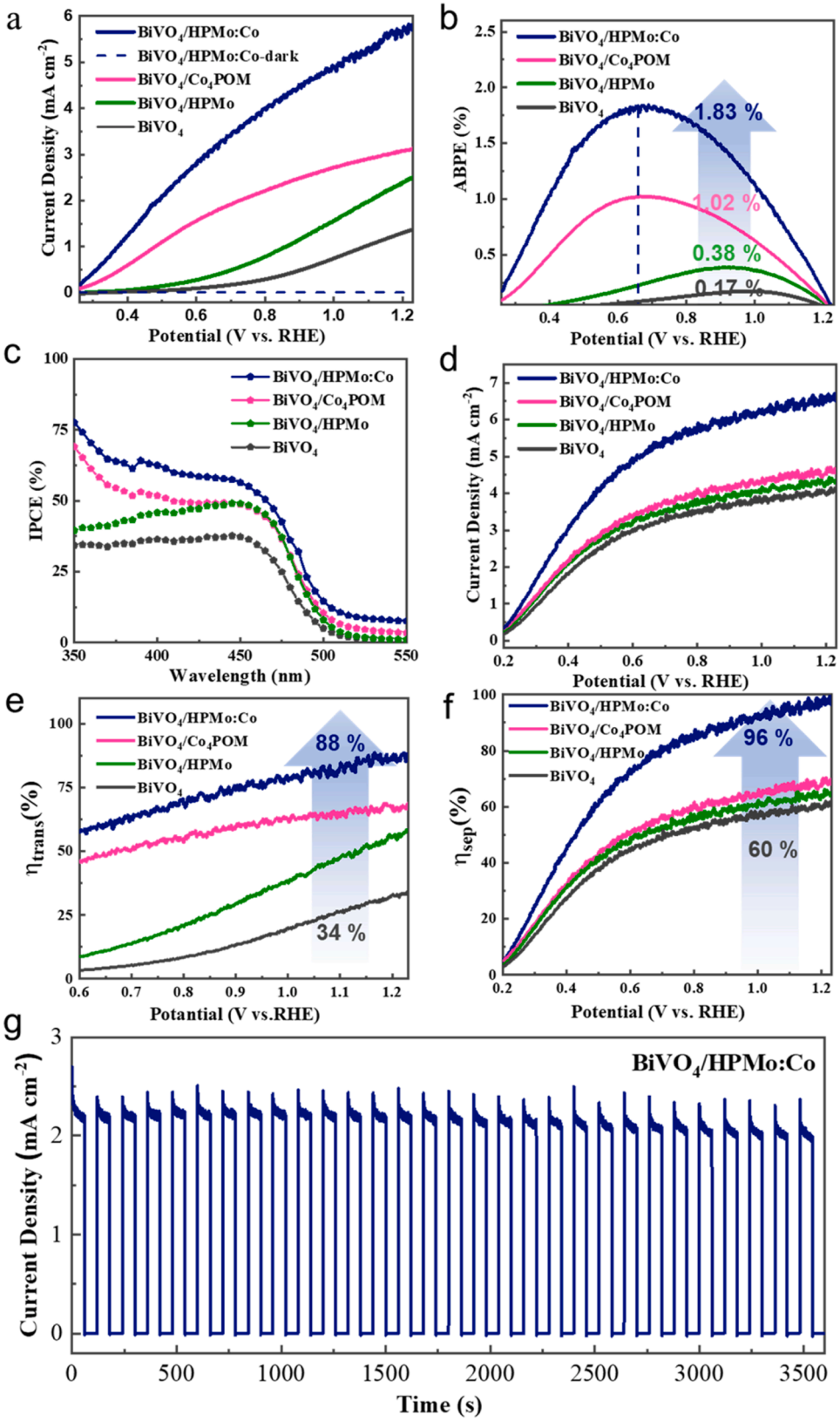

Fig. 3. PEC performance of various photoanodes. (a) Photocurrent density-potential curves. (b) ABPE curves. (c) IPCE curves. (d) Photocurrent density-potential curves in KBi electrolyte containing 0.2 M Na_2SO_3 under AM 1.5 G simulated sunlight (100 mW cm^{-2}). (e) Charge transfer efficiencies (η_{trans}). (f) Surface separation efficiency(η_{sep}). (h) Steady-state photocurrent density curve under chopped irradiation at 0.60 V vs. RHE.

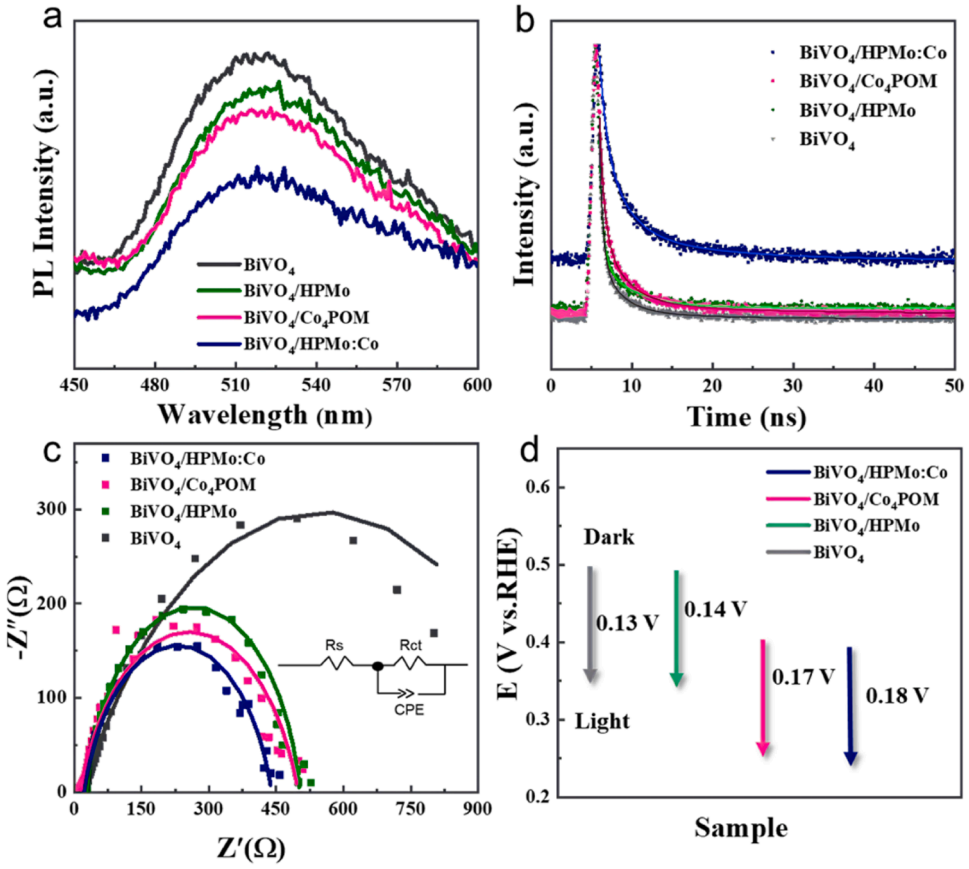

Fig. 4. (a) Steady-state photoluminescence spectra. (b) Time-resolved photoluminescence decay curves. (c) Electrochemical impedance spectroscopy curves. (d) The open circuit potential (OCP) transient decay profile.

and $BiVO_4$/Co_4POM (4.86 ns) photoanodes. This extended lifetime indicates that electron-hole recombination is effectively suppressed in the $BiVO_4$/HPMo: Co photoelectrode. The intensity modulated photocurrent and photovoltage spectroscopy (IMPS/IMVS) test (Figs. S6-8) was further confirmed that, $BiVO_4$/HPMo: Co photoanode owns the minimum electron collection time and the highest collection efficiency, the longest electron lifetime and average diffusion length. To further examine the electronic characteristics of the $BiVO_4$-based photoanodes,

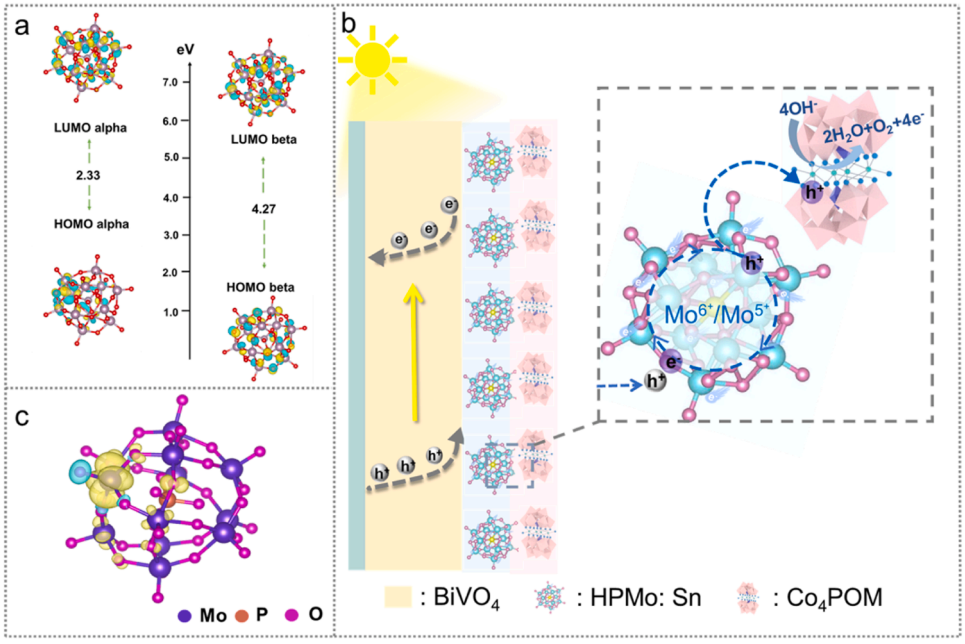

Fig. 5. (a) Molecular orbital diagram for HPMo: Sn. (b) Schematic diagram of PEC water oxidation mechanism of $BiVO_4$/HPMo: Co photoanode. (c) Computed Mulliken spin density distribution for HPMo: Sn.

we conducted electrochemical impedance spectroscopy (EIS) investigations [38]. Compared with other photoanodes, the $BiVO_4$/HPMo: Co photoanode exhibits the smallest charge transfer resistance, demonstrating that the HPMo: Sn HTL and the Co_4POM active layer substantially enhance the charge transfer reaction for surface water oxidation (Fig. 4c). The open-circuit photovoltage (OCP) values of all photoanodes are shown in Fig. 4d. Notably, the $BiVO_4$/HPMo: Co photoelectrode has the highest OCP increase, indicating that it possesses the highest driving force for water oxidation [39]. Based on the above analysis, the HPMo: Sn HTL and the Co_4POM catalyst demonstrate superior capabilities in promoting charge separation and extending carrier lifetimes.

To gain a comprehensive insight into the impact of the electronic structure of HPMO: Sn on the activity of the oxygen evolution reaction, we performed preliminary density functional theory (DFT) calculations. The DFT calculations performed at the PBE level, which accurately represents molecular orbitals. Fig. 5a illustrates the occupied and unoccupied molecular orbitals of HPMO: Sn. The lowest unoccupied molecular orbitals (LUMO) are basically contributed by Mo orbitals, and the bridging oxygen (O_b) and a small part of Mo orbitals contribute to the highest occupied orbitals (HOMO). The calculated values of the HOMO–LUMO gap for the alpha and beta spins are 2.33 eV and 4.27 eV, respectively. The average value of 3.30 eV is higher than the experimental value of 3.15 eV, attributed to the HOMO–LUMO gap being overestimated in the mixed functional [40]. Analysis by UV–vis absorption spectrum and TAUC diagram shows that the HOMO–LUMO energy difference of HPMO: Sn is 3.15 eV (Fig. S10a). For molecular compounds, the flat band potential closely aligns with the HOMO or LUMO energy [40]. From the positive slope of the Mott-Schottky plot in Fig. S10b, HPMO: Sn exhibits n-type behavior with a LUMO energy of 0.32 eV. Coupled with the HOMO–LUMO gap of 3.15 eV, the HOMO energy is 3.47 eV. The spin electron density distribution diagram of HPMO: Sn obtained by calculation (Fig. 5c) shows that the electrons of HPMO: Sn are mainly concentrated around Mo atoms. Combined with the fact that Mo atomic orbitals are the main contribution of LUMO, this provides evidence that the photogenerated holes primarily interact with the electrons surrounding Mo, and Mo^{6+}/ Mo^{5+} redox electron pairs serve as bridges for hole transport. In the absence of the Mo^{6+}/ Mo^{5+} hole transport bridge, HPMo and $SnCl_2$ alone could not exhibit any significant effect (Fig. S11). Based on the above data, the mechanism of the PEC water oxidation reaction occurring in the $BiVO_4$/HPMo: Co photoanode is inferred. During the PEC reaction, initially, the photogenerated holes generated by the $BiVO_4$ substrate preferentially recombine with electrons in the electron-rich heteropolyblue HPMO: Sn. Subsequently, the heteropolyblue HPMO: Sn, endowed with robust redox properties, undergoes self-cycling through the Mo^{6+}/ Mo^{5+} redox electron pair. This rapid regeneration of heteropolyblue HPMO: Sn replenishes consumed electrons and generates HOMO holes with higher positive potentials than the valence band of $BiVO_4$. Finally, the more oxidizing holes migrate to the Co_4POM active site to participate in the water oxidation reaction (Fig. 5b).

3. Conclusion

In summary, we present an isotropic water-soluble heteropolyblue HPMo: Sn HTL to break the limitations of traditional solid-phase HTL, thereby significantly improving the separation and transport efficiency of holes in the $BiVO_4$ photoanode. Coupling with cobalt-based polyoxometalates, the $BiVO_4$/HPMo: Co photoelectrode not only achieves a current density of 5.7 mA cm^{-2} at 1.23 V vs. RHE, but also exhibits an impressive charge separation efficiency of 96%. Combining computational and experimental results, we found that the Mo^{6*}/ Mo^{5*} pair in heteropolyblue acts as a bridge for hole transport. Furthermore, the electron-rich characteristics of heteropolyblue naturally attract holes, achieving the purpose of rapid separation of photogenerated electrons and holes. The robust redox properties of heteropolyblue confer durability to the HTL, ensuring the continuous conversion and transport of holes. This work exploits the potential of heteropolyblue as hole-transporting layers in PEC systems, providing novel perspectives into the development of straightforward and efficient PEC water splitting applications.

CRediT authorship contribution statement

Lei Gan: Methodology, Visualization, Investigation, Data curation, Writing – originaldraft. **GaoShuang He**: Data curation. **Yang Liu**: Supervision, Conceptualization. **Wenzhang Li**: Supervision, Conceptualization, Writing-review & editing. **Jie Li**: Writing – review & editing, Supervision, Conceptualization.

Declaration of Competing Interest

We have no known competing financial interests or personal relationships that could have appeared to influence the work reported in this paper.

Data availability

Data will be made available on request.

Acknowledgements

This study was supported by the Joint Funds of the National Natural Science Foundation of China (U22A20170) and the Fundamental Research Funds for the Central Universities of Central South University Project (2023ZZTS0069). This work was also supported in part by the High-Performance Computing Center of CentralSouth University.

Appendix A. Supporting information

Supplementary data associated with this article can be found in the online version at doi:10.1016/j.apcatb.2024.123895.

References

[1] Y.C. Miao, Z.H. Li, Y.J. Song, K. Fan, J. Guo, R.G. Li, M.F. Shao, Surface active oxygen engineering of photoanodes to boost photoelectrochemical water and alcohol oxidation coupled with hydrogen production, Appl. Catal. B Environ. 323 (2023) 122147.
[2] P.Y. Kuang, L.Y. Zhang, B. Cheng, J.G. Yu, Enhanced charge transfer kinetics of Fe_2O_3/CdS composite nanorod arrays using cobalt-phosphate as cocatalyst, Appl. Catal. B Environ. 218 (2017) 570–580.
[3] K.K. Wang, Y. Liu, K. Kawashima, X.T. Yang, X. Yin, F.Q. Zhan, M. Liu, X.Q. Qiu, W. Z. Li, C.B. Mullins, Modulating charge transfer efficiency of hematite photoanode with hybrid dual-metal–organic frameworks for boosting photoelectrochemical water oxidation, Adv. Sci. 7 (2020) 2002563.
[4] Z. Wu, X.Y. Liu, H.J. Li, Z.Y. Sun, M.S. Cao, Z.Z. Li, C.H. Fang, J.H. Zhou, C.B. Cao, J.C. Dong, S.L. Zhao, Z. Chen, A semiconductor-electrocatalyst nano interface constructed for successive photoelectrochemical water oxidation, Nat. Commun. 14 (2023) 2574.
[5] J. Zhang, H.P. Ma, Z.F. Liu, Highly efficient photocatalyst based on all oxides WO_3/Cu_2O heterojunction for photoelectrochemical water splitting, Appl. Catal. B Environ. 201 (2017) 84–91.
[6] A. Standing, S. Assali, L. Gao, M.A. Verheijen, D. Van Dam, Y. Cui, P.H. Notten, J. E. Haverkort, E.P. Bakkers, Efficient water reduction with gallium phosphide nanowires, Nat. Commun. 6 (2015) 7824.
[7] X.M. Zhang, P.L. Zhai, Y.X. Zhang, Y.Z. Wu, C. Wang, L. Ran, J.F. Gao, Z.W. Li, B. Zhang, Z.Z. Fan, L.C. Sun, J.G. Hou, Engineering single-atomic Ni-N_4-O sites on semiconductor photoanodes for high-performance photoelectrochemical water splitting, J. Am. Chem. Soc. 143 (2021) 20657–20669.
[8] J.G. Hou, C. Yang, H.J. Cheng, S.Q. Jiao, O. Takeda, H.M. Zhu, High-performance p-Cu_2 O/n-TaON heterojunction nanorod photoanodes passivated with an ultrathin carbon sheath for photoelectrochemical water splitting, Energy Environ. Sci. 7 (2014) 3758–3768.
[9] Y.B. Kuang, Q.X. Jia, G.J. Ma, T. Hisatomi, T. Minegishi, H. Nishiyama, M. Nakabayashi, N. Shibata, T. Yamada, A. Kudo, Ultrastable low-bias water splitting photoanodes via photocorrosion inhibition and in situ catalyst regeneration, Nat. Energy 2 (2016) 1–9.

[10] X.T. Xu, L. Pan, X. Zhang, L. Wang, J.J. Zou, Rational design and construction of cocatalysts for semiconductor-based photo-electrochemical oxygen evolution: a comprehensive review, Adv. Sci. 6 (2019) 1801505.
[11] W. Yang, R.R. Prabhakar, J. Tan, S.D. Tilley, J. Moon, Strategies for enhancing the photocurrent, photovoltage, and stability of photoelectrodes for photoelectrochemical water splitting, Chem. Soc. Rev. 48 (2019) 4979–5015.
[12] Y. Wang, D. Chen, J. Zhang, M.S. Balogun, P. Wang, Y. Tong, Y. Huang, Charge relays via dual carbon-actions on nanostructured $BiVO_4$ for high performance photoelectrochemical water splitting, Adv. Funct. Mater. 32 (2022) 2112738.
[13] X.X. Chang, T. Wang, P. Zhang, J.J. Zhang, A. Li, J.L. Gong, Enhanced surface reaction kinetics and charge separation of p–n heterojunction Co_3O_4/$BiVO_4$ photoanodes, J. Am. Chem. Soc. 137 (2015) 8356–8359.
[14] M. Zhou, J. Bao, Y. Xu, J.J. Zhang, J.F. Xie, M.L. Guan, C.L. Wang, L.Y. Wen, Y. Lei, Y. Xie, Photoelectrodes based upon Mo: $BiVO_4$ inverse opals for photoelectrochemical water splitting, ACS Nano 8 (2014) 7088–7098.
[15] M. Tayebi, B.-K. Lee, Recent advances in $BiVO_4$ semiconductor materials for hydrogen production using photoelectrochemical water splitting, Renew. Sustain. Energy Rev. 111 (2019) 332–343.
[16] M.A. Gaikwad, U.P. Suryawanshi, U.V. Ghorpade, J.S. Jang, M.P. Suryawanshi, J. H. Kim, Emerging surface, bulk, and interface engineering strategies on $BiVO_4$ for photoelectrochemical water splitting, Small 18 (2022) 2105084.
[17] X. Cheng, J.M. Wang, K. Zhao, Y.P. Bi, Spatially confined iron single-atom and potassium ion in carbon nitride toward efficient CO_2 reduction, Appl. Catal. B Environ. 316 (2022) 121643.
[18] M. Xiao, Z.L. Wang, B. Luo, S.C. Wang, L.Z. Wang, Enhancing photocatalytic activity of tantalum nitride by rational suppression of bulk, interface and surface charge recombination, Appl. Catal. B Environ. 246 (2019) 195–201.
[19] K. Zhang, B.J. Jin, C. Park, Y.J. Cho, X.F. Song, X.J. Shi, S.L. Zhang, W. Kim, H. Zeng, J.H. Park, Black phosphorene as a hole extraction layer boosting solar water splitting of oxygen evolution catalysts, Nat. Commun. 10 (2019) 2001.
[20] Š. Hajduk, S.P. Berglund, M. Podlogar, G. Dražić, F.F. Abdi, Z.C. Orel, M. Shalom, Conformal carbon nitride coating as an efficient hole extraction layer for ZnO nanowires-based photoelectrochemical cells, Adv. Mater. Interfaces 4 (2017) 1700924.
[21] Y.R. Song, X.M. Zhang, Y.X. Zhang, P.L. Zhai, Z.W. Li, D.F. Jin, J.Q. Cao, C. Wang, B. Zhang, J.F. Gao, L.C. Sun, J.G. Hou, Engineering MoO_x/MXene hole transfer layers for unexpected boosting of photoelectrochemical water oxidation, Angew. Chem. Int. Ed. 61 (2022) 202200946.
[22] G.J. Liu, J.Y. Shi, F.X. Zhang, Z. Chen, J.F. Han, C.M. Ding, S.S. Chen, Z.L. Wang, H. X. Han, C. Li, A tantalum nitride photoanode modified with a hole-storage layer for highly stable solar water splitting, Angew. Chem. Int. Ed. 53 (2014) 7295–7299.
[23] L. Ran, S. Qiu, P.L. Zhai, Z.W. Li, J.F. Gao, X.M. Zhang, B. Zhang, C. Wang, L. C. Sun, J.G. Hou, Conformal macroporous inverse opal oxynitride-based photoanode for robust photoelectrochemical water splitting, J. Am. Chem. Soc. 143 (2021) 7402–7413.
[24] N. Li, J. Liu, B.X. Dong, Y.Q. Lan, Polyoxometalate-based compounds for photo-and electrocatalytic applications, Angew. Chem. Int. Ed. 59 (2020) 20779–20793.
[25] J.J. Walsh, A.M. Bond, R.J. Forster, T.E. Keyes, Hybrid polyoxometalate materials for photo (electro-) chemical applications, Coord. Chem. Rev. 306 (2016) 217–234.
[26] F.R. Li, T. Wang, Y.J. Li, X.Y. Xu, C.H. Ma, W.L. Chen, G.S. Zhu, Heteropolyblue/protonation-defective graphitic carbon nitride heterojunction for the photo-driven nitrogen reduction reaction, Inorg. Chem. 60 (2021) 5829–5839.
[27] T. Wang, S.S. Qu, J.H. Wang, M. Xu, C.Q. Qu, M. Feng, W/Mo-heteropolyblue-modified defective $W_{18}O_{49}$ as Z-Scheme heterostructure photocatalysts for efficient N_2 fixation, J. Alloy. Compd. 938 (2023) 168631.
[28] Q. Kang, Z. Zheng, Y.F. Zu, Q. Liao, P.Q. Bi, S.Q. Zhang, Y. Yang, B.W. Xu, J. H. Hou, n-doped inorganic molecular clusters as a new type of hole transport material for efficient organic solar cells, Joule 5 (2021) 646–658.
[29] Q. Sun, T. Cheng, Z.R. Liu, L. Qi, A cobalt silicate modified $BiVO_4$ photoanode for efficient solar water oxidation, Appl. Catal. B Environ. 277 (2020) 119189.
[30] S.D. Adhikary, A. Tiwari, T.C. Nagaiah, D. Mandal, Stabilization of cobalt-polyoxometalate over poly (ionic liquid) composites for efficient electrocatalytic water oxidation, ACS Appl. Mater. Interfaces 10 (2018) 38872–38879.
[31] H. Xin, L. Lin, R.T. Li, D. Li, T.Y. Song, R.T. Mu, Q. Fu, X.H. Bao, Overturning CO_2 hydrogenation selectivity with high activity via reaction-induced strong metal–support interactions, J. Am. Chem. Soc. 144 (2022) 4874–4882.
[32] Y. Choi, D. Jeon, Y. Choi, D. Kim, N. Kim, M. Gu, S. Bae, T. Lee, H.-W. Lee, B.-S. Kim, Interface engineering of hematite with nacre-like catalytic multilayers for solar water oxidation, ACS Nano 13 (2018) 467–475.
[33] X.T. Yang, J.P. Cui, L.X. Lin, A. Bian, J. Dai, W. Du, S.Y. Guo, J.G. Hu, X.Y. Xu, Enhanced charge separation in nanoporous $BiVO_4$ by external electron transport layer boosts solar Water splitting, Adv. Sci. (2023) 2305567.
[34] Z.Z. Zhang, X.J. Huang, B.B. Zhang, Y.P. Bi, High-performance and stable $BiVO_4$ photoanodes for solar water splitting via phosphorus–oxygen bonded FeNi catalysts, Energy Environ. Sci.. 15 (2022) 2867–2873.
[35] G.J. Dong, L.L. Yan, Y.P. Bi, Advanced oxygen evolution reaction catalysts for solar-driven photoelectrochemical water splitting, J. Mater. Chem. A 11 (2023) 3888–3903.
[36] B.Y. Liu, X. Wang, Y.J. Zhang, L.C. Xu, T.S. Wang, X. Xiao, S.C. Wang, L.Z. Wang, W. Huang, A $BiVO_4$ photoanode with a VO_x layer bearing oxygen vacancies offers improved charge transfer and oxygen evolution kinetics in photoelectrochemical water splitting, Angew. Chem. Int. Ed. 62 (2023) e202217346.
[37] L. Gan, H. Mei, Q.Z. Lin, J.L. Peng, X.F. Ji, R.B. Zhang, X.W. Wang, Three-dimensionally ordered Macroporous perovskite sodium tantalum for robust hydrogen and hydrogen peroxide production, J. Colloid Interface Sci. 613 (2022) 597–605.
[38] X.W. Wang, L. Gan, Q.Z. Lin, S. Ye, R.B. Zhang, J. Liu, Micro-terminal regulation in nanoreactors for the construction of tantalum pentoxide single-crystal ordered networks with promoting enhanced hydrogen evolution performance, Chem. Eng. J. 431 (2022) 134139.
[39] Y. Zhong, C.L. Wu, X.F. Jia, S.J. Sun, D.M. Chen, W.Q. Yao, H. Ding, J.Y. Zhang, T. Y. Ma, Coupling of self-healing atomic layer CoAl-LDH onto Mo: $BiVO_4$ photoanode for fast surface charge transfer toward stable and high-performance water splitting, Chem. Eng. J. 465 (2023) 142893.
[40] G.Y. Zhang, M. Baranov, F. Wang, J.M. Poblet, S. Kozuch, N. Leffler, A.I. Shames, J. M. Clemente-Juan, A. Neyman, I.A. Weinstock, Soluble complexes of cobalt oxide fragments bring the unique CO_2 photoreduction activity of a bulk material into the flexible domain of molecular science, J. Am. Chem. Soc. 143 (2021) 20769–20778.